

1 **BrGDGTs-based seasonal paleotemperature reconstruction for the last 15,000 years from**  
2 **a shallow lake on the eastern Tibetan Plateau**

3 Xiaohuan Hou <sup>a</sup>, Nannan Wang <sup>a</sup>, Zhe Sun <sup>b</sup>, Kan Yuan <sup>a,c</sup>, Xianyong Cao <sup>a</sup>, Juzhi Hou <sup>a\*</sup>

4 <sup>a</sup> *Group of Alpine Paleocology and Human Adaptation (ALPHA), State Key Laboratory of Tibetan*  
5 *Plateau Earth System, Resources and Environment (TPESRE), Institute of Tibetan Plateau Research,*  
6 *Chinese Academy of Sciences, Beijing 100101, China*

7 <sup>b</sup> *Institute of Geography and Resources Science, Sichuan Normal University, Chengdu, 610066, China*

8 <sup>c</sup> *University of Chinese Academy of Sciences, Beijing 100049, China*

9

10 \* Corresponding author

11 E-mail address: houjz@itpcas.ac.cn

12

13 **ABSTRACT**

14 Understanding Holocene temperature changes is vital for resolving discrepancies between  
15 proxy reconstructions and climate models. The intricate temperature variations across the  
16 Tibetan Plateau (TP) add complexity to studying continental climate change during this  
17 period. Discrepancies between model-based and proxy-based reconstructions might stem  
18 from seasonal biases and environmental uncertainties in the proxies. Employing multiple  
19 proxies from a single sediment core for quantitative temperature reconstructions offers an  
20 effective method for cross-validation in terrestrial environments. Knowledge of Holocene  
21 temperature changes is crucial for addressing the problem of the discrepancy between  
22 Holocene proxy temperature reconstructions and climate model simulations. The complex  
23 spatiotemporal pattern of temperature variations on the Tibetan Plateau (TP) further  
24 complicates the study of Holocene continental climate change. The discrepancy between  
25 model-based and proxy-based Holocene temperature reconstructions possibly results from the  
26 seasonal biases and environmental ambiguities of the proxies. Quantitative temperature  
27 reconstructions using different proxies from the same sediment core can provide an effective  
28 means of evaluating different proxies; however, this approach is unusual in terrestrial  
29 environments. Here, we present an ice-free-season temperature record for the past 15 ka from  
30 a shallow, freshwater lake on the eastern TP, based on brGDGTs (branched glycerol dialkyl  
31 glycerol tetraethers). This record shows that the Holocene Thermal Maximum lags the  
32 pollen-based July temperature recorded in the same sediment core. We conclude that the  
33 mismatch between the brGDGTs-based and pollen-based temperatures is primarily the result  
34 of seasonal variations in solar irradiance. The overall pattern of temperature changes is

35 supported by other summer temperature records, and the Younger Dryas cold event and the  
36 Bølling–Allerød warm period are also detected. A generally warm period occurred during 8–  
37 3.5 ka, followed [by a cooling trend](#) in the late Holocene. Our findings have implications for  
38 understanding the seasonal signal of brGDGTs in shallow lakes, and provide critical data for  
39 confirming the occurrence of seasonal biases in different proxies from high–elevation lakes.  
40 To further investigate the significance of the brGDGTs and temperature patterns on the TP,  
41 [we examined existing brGDGTs-based Holocene temperature records, which interpret these](#)  
42 [compounds as indicators of mean annual or growing season temperatures. we reviewed](#)  
43 [previously published brGDGTs-based Holocene temperature records across the TP. In these](#)  
44 [studies, brGDGTs have been interpreted to reflect either mean annual air temperature or](#)  
45 [growing season temperature. In both cases, brGDGTs reflect a gradual warming trend during](#)  
46 [the Holocene with relatively cooler conditions during the middle Holocene, and a cooling](#)  
47 [trend during the middle to late Holocene. The existing/available temperature records show](#)  
48 [complicated patterns of variation, some with general warming trends throughout the](#)  
49 [Holocene, some with cooling trends, while some with warm middle Holocene.](#) We analyzed  
50 the possible reasons for the diverse brGDGTs records on the TP and emphasize the  
51 importance of considering lake conditions and modern investigations of brGDGTs in  
52 lacustrine systems when using brGDGTs to reconstruct paleoenvironmental conditions.

53 **Keywords:** Tibetan Plateau, brGDGTs, the mean temperature of Months Above Freezing,  
54 shallow lake, Holocene

## 55 **1 Introduction**

56 Global climate change has [had](#) a profound impact on both the natural ecological and socio-

57 economic systems that are vital for human survival and development, making climate change  
58 a critical limiting factor for the sustainable development of human society. The Tibetan Plateau  
59 (TP), also called the “Third Pole” (Qiu, 2008), has undergone a more rapid warming over the  
60 last five decades, with a rate twice that of the global average (0.3 – 0.4°C/decade) (Kuang and  
61 Jiao, 2016; Chen et al., 2015), making it one of the world's most temperature-sensitive regions  
62 (Chen et al., 2015; Yao et al., 2022). Consequently, assessing the impact of future climate  
63 change on the TP is becoming increasingly important. To enhance the precision and accuracy  
64 of future climate change estimates for the TP under ongoing global climate change and to  
65 minimize the uncertainty in climate simulations, it is essential to investigate the processes and  
66 mechanisms of regional climate and environmental changes, with particular emphasis on  
67 temperature, on a relatively long timescale, such as that of the Holocene.

68  
69 The Holocene, the most recent geological epoch, is closely linked with the development of  
70 human civilization. Quantitative reconstructions of Holocene temperature trends can be used  
71 to explore their impacts on civilization and to establish a geological and historical context for  
72 predicting future climate changes. In recent decades, many Holocene quantitative  
73 reconstructions of seasonal and annual temperatures for the TP have been produced using  
74 various proxies, like pollen (Herzschuh et al., 2014; Lu et al., 2011), chironomids (Zhang et al.,  
75 2017; Zhang et al., 2019a),  $\delta^{18}\text{O}$  in ice cores (Pang et al., 2020; Thompson et al., 1997), and  
76 biomarkers (Hou et al., 2016; Zhao et al., 2013; Cheung et al., 2017). These reconstructions  
77 have provided crucial data for the elucidation of Holocene temperature changes. However, the  
78 available Holocene temperature records from the TP show divergent trends. Multiple proxy  
79 indicators indicate three different Holocene temperature patterns on the TP. First, a consistent

80 Holocene warming trend (Sun et al., 2022; Feng et al., 2022; Opitz et al., 2015). For example,  
81 brGDGTs based annual temperatures (Feng et al., 2022; Sun et al., 2022) indicate a gradual  
82 warming trend which resembles the  $\delta^{18}\text{O}$  temperature record from the Chongce ice core on the  
83 western TP, except for the last 2 ka (Pang et al., 2020). Second, an early to middle Holocene  
84 summer temperature maximum and a gradual cooling trend during the late Holocene are  
85 observed in pollen-, alkenone- and chironomid-based temperature records (Herzschuh et al.,  
86 2014; Hou et al., 2016; Zhang et al., 2017; Wang et al., 2021a; Zheng et al., 2015). Third, a  
87 prominent relatively cool middle Holocene (Wang et al., 2021c; Li et al., 2017); for example,  
88 a composite temperature record suggests that temperatures were  $\sim 2^\circ\text{C}$  cooler during the middle  
89 Holocene than during the early and late Holocene (Wang et al., 2021c). Several records also  
90 show a steady long-term trend without distinct cooling or warming (Sun et al., 2021). Moreover,  
91 the cooling trends in proxy-based Holocene temperature records are inconsistent with those of  
92 climate models, which indicate a warming trend, and this inconsistency is widely known as the  
93 “Holocene temperature conundrum” (Liu et al., 2014). There are several potential factors that  
94 may contribute to the disparity in Holocene temperature trends, including seasonal biases and  
95 uncertainties in temperature proxies and reconstructions, independent of climate models (Liu  
96 et al., 2014; Hou et al., 2019; Bova et al., 2021; Cartapanis et al., 2022; Marsicek et al., 2018).  
97 While several recent studies have suggested that seasonality in proxies is not the major cause  
98 of the Holocene temperature conundrum (Dong et al., 2022; Zhang et al., 2022b), it is  
99 significant that the TP is an alpine and high-altitude region with significant seasonal  
100 temperature variations. Moreover, most organisms tend to grow during the warmer seasons at  
101 high latitudes and high altitudes (Zhao et al., 2021a). Currently, however, we lack unambiguous

102 and reliable seasonal temperature records to support a seasonality-bias hypothesis. Extensive  
103 research has been conducted in lakes, employing a single proxy to reconstruct past temperature  
104 fluctuations. However, there have been scarce studies that employ various proxies within the  
105 same core to reconstruct paleotemperature variations. Furthermore, the limited number of  
106 studies primarily concentrate on reconstructing summer temperature and annual average  
107 temperature. For example, a chironomid-based July temperature reconstruction for Tiancai lake  
108 on the southeastern TP shows higher temperatures during the early to middle Holocene ([Zhang  
109 et al., 2017](#)), while the brGDGTs-based annual average temperature shows a warming trend  
110 ([Feng et al., 2022](#)). Different proxies may reflect the seasonal temperatures in different months,  
111 and thus producing temperature reconstructions for different months for the same sediment  
112 core may help better understand the seasonal bias of terrestrial temperature records.  
113 Furthermore, the reconciliation of the divergent trends of Holocene temperature on the TP and  
114 its surroundings requires additional high-altitude temperature records from these regions, with  
115 reliable chronologies and proxy records with an unambiguous climatological significance.

116  
117 Branched glycerol dialkyl glycerol tetraethers (brGDGTs) are a group of membrane-spanning  
118 lipids found in bacteria (Fig. S1) ([Chen et al., 2022](#); [Halamka et al., 2022](#); [Sinninghe Damsté  
119 et al., 2000](#)), and they have become a powerful tool for quantifying past terrestrial temperature  
120 variations. Through investigations of brGDGTs in globally-distributed soils, it was found that  
121 the distribution of brGDGTs is primarily related to temperature and pH ([Weijers et al., 2007](#)).  
122 Subsequently, brGDGTs–temperature calibrations from soil, peat and lake sediments were  
123 established on scales from global ([Weijers et al., 2007](#); [De Jonge et al., 2014](#); [Crampton-Flood](#)

124 et al., 2020; Martínez-Sosa et al., 2021) to regional (e.g., East Asia) (Sun et al., 2011; Ding et  
125 al., 2015; Wang et al., 2016; Dang et al., 2018), leading to considerable progress in  
126 reconstructing terrestrial temperatures, particularly on the TP (Cheung et al., 2017; Zhang et  
127 al., 2022a; Li et al., 2017).

128

129 Natural lakes are widely distributed across the TP (Zhang et al., 2019b). Lake sediments,  
130 characterized by their organic matter-rich composition, exhibit continuous and rapid  
131 accumulation rates. As a result, they offer high-resolution records of environmental changes,  
132 making them highly valued as a primary terrestrial climate archive (Moser et al., 2019).  
133 BrGDGTs in lacustrine systems are often more strongly correlated with temperature, with  
134 higher coefficient of determination ( $r^2$ ) and lower root mean square error (RMSE) values  
135 (Martínez-Sosa et al., 2021), than in soils and peats. Nevertheless, the factors that impact the  
136 distribution of brGDGTs in lakes are intricate and multidimensional. Notably, the sources of  
137 brGDGTs within lakes are intricate, involving contributions from soil as well as autochthonous  
138 lake processes. However, an expanding body of research underscores a substantial prevalence  
139 of autochthonous brGDGTs in lakes (Tierney and Russell, 2009; Tierney et al., 2010; Weber et  
140 al., 2015; Wang et al., 2021b). Furthermore, the origins of brGDGT producers remain uncertain  
141 and could be influenced by various factors, including lake salinity (Wang et al., 2021b), redox  
142 conditions (Weber et al., 2018), oxygen content and/or mixing patterns (Van Bree et al., 2020;  
143 Wu et al., 2021; Buckles et al., 2014). Additionally, even lake depth plays a role due to distinct  
144 ecological niches (Woltering et al., 2012), thereby contributing to the intricate interplay that  
145 shapes the distribution of brGDGTs within lakes.

146

147 In this study, we obtained a quantitative temperature reconstruction for the past 15 ka from  
148 Gahai, a shallow (average depth of ~2 m) freshwater lake located in the source area of the  
149 Yellow River. This region is an important ecological protection area on the eastern edge of the  
150 TP. Freshwater environments avoid the confounding effects of salinity on brGDGTs-based  
151 temperature reconstructions, and shallow lakes also minimize the impact of the uneven  
152 distribution of light and nutrients on brGDGTs. Our specific aims were: (1) to determine the  
153 long-term trend of Holocene warm-biased terrestrial temperatures at a high elevation; (2) to  
154 compare records of ice-free season temperatures with July temperatures from the same  
155 sediment core; and (3) to gain a better understanding of the possible mechanisms responsible  
156 for Holocene temperature variations, especially on the TP.

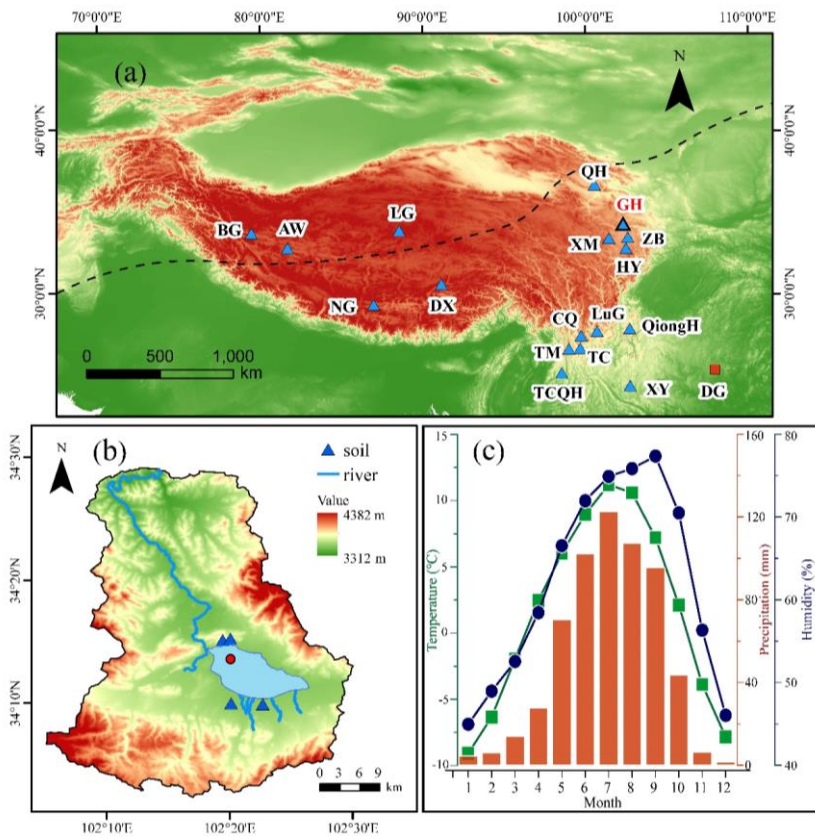
## 157 **2 Materials and methods**

### 158 *2.1 Study site*

159 Gahai (102°11'–102°28' E, 34°04'–34°4' N, 3444 m a.s.l.) is a freshwater lake and part of the  
160 Gahai meadow wetland, which is a national nature reserve with restricted human access, on the  
161 eastern edge of the Tibetan Plateau (Fig. 1). The lake is fed by runoff from the surrounding  
162 hills, drains into the Tao River, and ultimately enters the Yellow River. Thus, Gahai lake is a  
163 critical water conservation area in the upper reaches of the Yellow River. The average water  
164 depth of Gahai is ~1–2 m, and the maximum depth is ~5 m. The vegetation in the catchment  
165 consists mainly of *Kobresia tibetica*, *Equisetum arvense*, *Potentilla anserina*, *Artemisia*  
166 *subulate*, and *Oxytropis falcata* (Ma et al., 2019). Meteorological data for the area are available  
167 from Langmu Temple station (1957-1988) (Fig. 1) (102°38' E, 34°5' N, 3412 m a.s.l.), ~32 km



168 northwest of Gahai lake. They indicate an annual average (mean) precipitation of 781 mm,  
 169 with > 67% occurring between June and September, and mean annual temperature of 1.2 °C  
 170 with a relative humidity of ~65%. The summers are mild and humid and the winters are cold  
 171 and dry. From May to September, the mean average temperature is above freezing (0°C), but  
 172 the temperature in May is very low, close to 0°C.



173  
 174 **Fig. 1** (a) Locations of the sites on the Tibetan Plateau referenced in the text. Triangle with  
 175 bold line indicates the location of Gahai lake (this study). Other triangles indicate the  
 176 locations of cited studies on the Tibetan Plateau and the surrounding area: Bangong Co  
 177 (BG), Aweng Co (AW), Ngamring Co (NG), Linggo Co (LG), Dangxiong wetland (DX),

178 Qinghai lake (QH), Ximen Co (XM), Zoige Basin (ZB), Hongyuan peatland (HY), Lugu  
179 lake (LuG), Cuoqia lake (CQ), Tingming lake (TM), Tengchongqinghai lake (TCQH),  
180 Tiancai lake (TC), Qionghai lake (QH), Xingyun lake (XY). Red square indicates  
181 Dongge Cave (DG). Black dotted line represents the northern boundary of the modern  
182 Asian summer Monsoon (Chen et al., 2008). (b) Drainage basin of Gahai lake and the  
183 core site. (c) Climate data from Langmu Temple meteorological station: monthly  
184 temperature (green line), precipitation (red bars), and humidity (blue line).

## 185 2.2 Sampling

186 A sediment core with the length of 329 cm was obtained from Gahai Lake in January 2019, at  
187 a water depth of 1.95 m, using a UWITEC platform operated from the frozen lake surface. In  
188 addition, four catchment soil samples were collected from around the lake (Fig. 1). All samples  
189 were transported to the Institute of Tibetan Plateau Research, Chinese Academy of Sciences  
190 (ITPCAS). The sediment core was split lengthwise, and one half was subsampled and freeze-  
191 dried for subsequent analysis.

192

## 193 2.3 Chronology

194 The chronology of the upper 20 cm of the sediment core is based on measurements of  $^{210}\text{Pb}$   
195 and  $^{137}\text{Cs}$ , at a 1-cm interval. The chronology for the deeper part of the core is provided by  
196 accelerator mass spectrometry (AMS)  $^{14}\text{C}$  measurements of 13 bulk sediment samples, which  
197 were conducted by Beta Analytic Inc. (Miami, USA) (Fig. 2) (Wang et al., 2022).

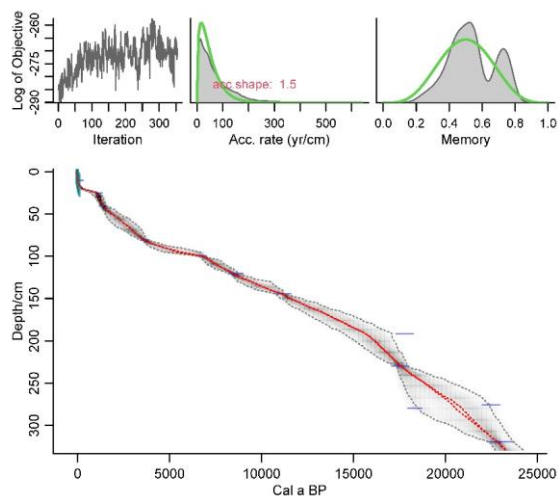
198

199 The  $^{210}\text{Pb}$  age model was constructed using the constant rate of supply (CRS) model and the  
200  $^{137}\text{Cs}$  peak was used as supplement (Appleby, 2002). The calculated age of  $^{210}\text{Pb}$  using CRS  
201 model aligned well with the  $^{137}\text{Cs}$  peak at 6 cm. Overall, the CRS model was deemed suitable

202 for determining the age of Gahai lake.

203

204 Reservoir age, as highlighted by Hou et al. (2012), is a crucial factor affecting the age  
205 determination of lake sediment cores on the TP. Therefore, it was necessary to establish the  
206 reservoir age of Gahai lake before undertaking paleoclimate reconstruction. The linear  
207 extrapolation relationship between the  $^{14}\text{C}$  ages and depth to the sediment-water interface is  
208 often used to estimate the reservoir age. The  $^{14}\text{C}$  age of 13 samples exhibits a good linear  
209 relationship with sediments depth in Gahai lake. Extrapolation of this 13  $^{14}\text{C}$  ages down to the  
210 depth of 6 cm yielded a  $^{14}\text{C}$  age of 461 yr BP, while the reliable  $^{210}\text{Pb}$  age at 6 cm is -27 yr BP.  
211 Consequently, the difference between the two ages, which amounts to 488 yr, was taken as the  
212 reservoir age. Additionally, it's worth noting that independent estimations of the  $^{14}\text{C}$  calibration  
213 age and  $^{210}\text{Pb}$  age around 10 cm in Gahai lake was obtained, resulting in values of 497 yr BP  
214 and 18 yr BP, respectively. The difference of 479 yr between these two ages can also be  
215 considered as the reservoir age. These two methods of estimating reservoir age of Gahai lake  
216 show very close, which are mutually supportive. So, the average of 483 yr was adopted as the  
217 reservoir age. All original  $^{14}\text{C}$  dates were corrected by subtracting the reservoir age (483 yr)  
218 and calibrating them to calendar ages using Calib 8.1. The age-depth model (Fig. 2) was  
219 constructed using the Bacon program with the  $^{14}\text{C}$  ages and  $^{210}\text{Pb}$  ages (Blaauw and Andres  
220 Christen, 2011) and was reported by Wang et al. (2022).



221 **Fig. 2** Age-depth model for Gahai, based on AMS  $^{14}\text{C}$ ,  $^{210}\text{Pb}$  and  $^{137}\text{Cs}$  ages (Wang et al.,  
 222 2022). The ages of the upper 20 cm are based on  $^{210}\text{Pb}$  and  $^{137}\text{Cs}$  dating (green symbols)  
 223 and those of the lower part on AMS  $^{14}\text{C}$  dates (blue symbols).  
 224

225

#### 226 2.4 Lipids extraction and brGDGTs analysis

227 For lipids extraction, ~5 g samples were ground to a powder and extracted ultrasonically with  
 228 dichloromethane (DCM): methanol (MeOH) (9: 1, v: v) three times. The supernatants were  
 229 combined and dried under a stream of nitrogen gas. Subsequently, the total lipid extracts were  
 230 separated into neutral and acid fractions through a LC-NH<sub>2</sub> silica gel column using DCM:  
 231 isopropyl alcohol (2: 1, v: v) and ether with 4% acetic acid (v: v), respectively. The neutral  
 232 fraction was then eluted through a silica gel column using n-Hexane, DCM and MeOH, and  
 233 the GDGTs were dissolved in the MeOH. The GDGTs fraction was passed through a 0.45 μm  
 234 polytetrafluoroethylene (PTFE) filter before analysis. C<sub>46</sub>-GDGT (a standard compound)  
 235 (Huguet et al., 2006) was added to the samples before analysis.

236

237 BrGDGTs were detected using an HPLC-APCI-MS (Waters ACQUITY UPLC I-Class/Xevo  
238 TQD) with auto-injection at the ITPCAS. The compounds were separated by three Hypersil  
239 Gold Silica LC columns in sequence (each 100 mm × 2.1 mm, 1.9 μm, Thermo Fisher Scientific;  
240 USA), maintained at a temperature of 40°C. GDGTs were eluted isocratically using 84%  
241 hexane and 16% ethyl acetate (EtOA) for the first 5 min, followed by a linear gradient change  
242 to 82% hexane and 18% EtOA from 5 to 65 min. The columns were cleaned using 100% EtOA  
243 for 10 min, and then back to 84% hexane and 16% EtOA to equilibrate the column, with a flow  
244 rate of 0.2 ml min<sup>-1</sup>.

245

246 The APCI-MS conditions were as follows: nebulizer pressure at 60 psi, APCI probe  
247 temperature at 400°C, drying gas flow rate of 6 L/min and temperature of 200°C, capillary  
248 voltage of 3600 V, source corona of 5.5 μA. Detection was performed in selected ion  
249 monitoring (SIM) mode, targeting the protonated molecules at m/z 1050, 1048, 1046, 1036,  
250 1034, 1032, 1022, 1020, 1018 and 744. The results were analyzed using MassLynx V4.1  
251 software, and quantification was achieved by comparing the peak areas of targeted ions and the  
252 internal standard, assuming an identical response factor for GDGTs.

253

### 254 **3 Results and Discussion**

#### 255 *3.1. Concentration and distribution of brGDGTs in the sediment core and catchment soils*

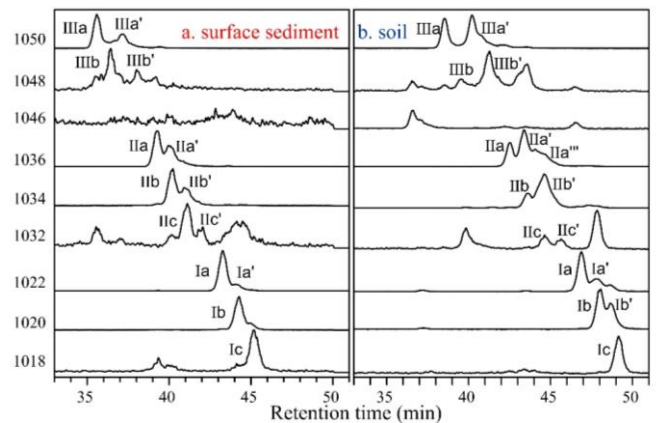
256 BrGDGTs were detected in both the catchment soils and the downcore sediments. The average  
257 concentration of brGDGTs in the catchment soils (0.07 ng g<sup>-1</sup>dw) was lower than in the surficial  
258 core sediments (0.70 ng g<sup>-1</sup>dw). In the soil samples, pentamethylated brGDGTs were generally

259 the most abundant (55.33%), followed by tetramethylated brGDGTs (23.60%) and  
260 hexamethylated brGDGTs (21.07%) (Fig. S2). The relative amount of cyclopentane ring-  
261 containing brGDGTs in the soil samples was generally low (24.34%) and it was sometimes too  
262 low to be detected, especially the fractions of IIIb, IIIb', IIIc, IIIc', IIc and IIc'. In the downcore  
263 sediments, the relative abundant of tetramethylated brGDGTs (43.84%) was like that of  
264 pentamethylated brGDGTs (41.93%), and hexamethylated brGDGTs were the least abundant  
265 (14.22%) (Fig. S2). The relative abundant of cyclopentane ring-containing brGDGTs in the  
266 downcore sediments (67.82%) was lower than that in the catchment soils.

### 267 3.2 *In situ* production of brGDGTs in Gahai lake

268 Although lacustrine brGDGTs have great potential for quantitatively reconstructing terrestrial  
269 paleotemperatures, uncertainties about their sources in lacustrine environments are a major  
270 factor limiting their application (Tierney and Russell, 2009; Cao et al., 2020; Sun et al., 2011;  
271 [Sinninghe Damsté et al., 2009](#); [Buckles et al., 2014](#)). To investigate the origin and  
272 characteristics of brGDGTs in the Gahai lake sediments, we examined the distributions and  
273 concentrations of brGDGTs in the sediments and catchment soils and found notable differences  
274 between them. First, as described in the previous section, the average content of brGDGTs in  
275 the catchment soils was ~10% that of the surficial lake sediments, suggesting the absence of  
276 large-scale allochthonous inputs from the catchment soils. Second, the brGDGTs distributions  
277 in the downcore sediments were quite different from those in the catchment soils, which  
278 suggests a substantial autochthonous brGDGTs contribution to the lake sediments (Fig. 3 and  
279 Fig. S2). Moreover, the ratios of 6-methyl brGDGTs to 5-methyl GDGTs ( $IR_{6ME}$ ) in the soils  
280 and sediments, calculated according to the formula proposed by [De Jonge et al. \(2014\)](#), were

281 different. In the soil samples, IR<sub>6ME</sub> varied between 0.54 and 0.57 and the average ratio in the  
 282 downcore samples was 0.26, varying between 0.18 and 0.47. Third, the in-situ production of  
 283 brGDGTs in Gahai lake is suggested by the discrepancies in the degree of methylation  
 284 (MBT'<sub>5ME</sub>) between the soils and surface sediments. The average value of MBT'<sub>5ME</sub> in the  
 285 Gahai lake surface sediments was 0.48, which is clearly higher than in the catchment soils,  
 286 with the range of 0.32–0.35. Fourth, and potentially the most significant, the IIIb' and Ib'  
 287 compounds are present in the catchments soil but not in the Gahai lake surficial sediments,  
 288 which may be direct evidence of an autochthonous brGDGTs contribution in the lacustrine  
 289 environment (Fig. 3), and a lower proportion of soil-derived brGDGTs input. Therefore, we  
 290 conclude that the brGDGTs in the Gahai lake sediments are mainly of in-situ origin.



291  
 292 **Fig. 3** Representative high-performance liquid chromatography/atmospheric pressure  
 293 chemical ionization-mass spectrometry (HPLC/APCIMS) chromatograms of brGDGTs  
 294 from (a) surface sediments from Gahai lake, and (b) soils in the catchment of Gahai  
 295 lake.

296

297 *3.3 brGDGTs-temperature calibration and Holocene temperature reconstruction*

298 Gahai is a shallow lake in the eastern Tibetan Plateau that is typically completely frozen during  
299 winter and spring. Local meteorological data indicate that the average snowfall period lasts for  
300 269 days, with around 50 days of continuous snowfall ([Luqu County Local Chronicles](#)  
301 [Compilation Committee, 2006](#)). The freezing of the lake surface begins in late October each  
302 year and gradually thaws starting from May of the following year. As a result, the light  
303 transmittance and oxygen content in the lake water are reduced during the freezing season,  
304 leading to decreased nutrient levels, which severely hinder the growth of autotrophic  
305 microorganisms. Although the bacteria responsible for producing brGDGTs have not been  
306 thoroughly characterized, the abundance of heterotrophic bacteria will likely decrease due to  
307 the reduced autotrophic biomass during the winter and spring ice-covered period. The  
308 weakened light penetration, decreased oxygen levels, and lack of nutrient replenishment during  
309 the frozen period significantly impact the growth of autochthonous microorganisms.

310  
311 Furthermore, some research suggests that the production of brGDGTs might be related to  
312 factors such as water depth, seasonal alternation of water column mixing and stratification  
313 ([Loomis et al., 2014](#); [Van Bree et al., 2020](#)). During the summer and autumn seasons when the  
314 lake ice melts and the water becomes more mobile, the nutrient content increases, resulting in  
315 elevated lake biomass, moreover, the oxygen levels at the bottom of Gahai lake are not expected  
316 to be too high, which could further contribute to the proliferation of brGDGT-producing  
317 bacteria, potentially leading to an increase in the brGDGT-producing bacteria ([Weber et al.,](#)  
318 [2018](#)). Therefore, brGDGTs in Gahai lake may provide records of the average temperature



319 during the ice-free months of the summer and autumn seasons.

320

321 Additionally, the presence of the frozen lake surface during winter creates a thermal barrier,  
322 impeding the exchange of heat between the lake water and the atmosphere. Consequently, any  
323 brGDGTs generated within the lake water during this period lose their ability to accurately  
324 reflect atmospheric temperature variations (Sun et al., 2021; Zhang et al., 2022a). Thus, they  
325 were no longer able to track atmospheric temperature changes during the frozen season. So, we  
326 prefer to use Gahai brGDGTs to reconstruct temperatures during the summer and ice-free  
327 seasons. For this purpose, we employed the new Bayesian calibration for the mean temperature  
328 of the Months Above Freezing (MAF), as proposed by Martínez-Sosa et al. (2021), to derive a  
329 MAF for Gahai lake.

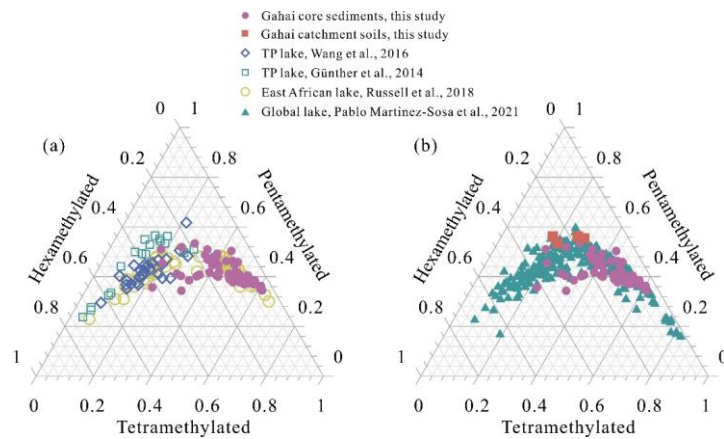
330

331 To assess the accuracy of this calibration approach, we compared the fractional abundances of  
332 summed tetra-, penta-, and hexamethylated brGDGTs in Gahai lake sediments with other  
333 datasets (Fig. 4). These datasets include lake sediments from the Tibetan Plateau (Günther et  
334 al., 2014; Wang et al., 2016), East Africa (Russell et al., 2018), and global lakes (Martínez-  
335 Sosa et al., 2021). The distribution pattern of Gahai core sediments is distinctly remarkable  
336 compared to that of other lake sediments within the Tibetan Plateau, even though they share a  
337 common regional origin (Fig. 4). However, its resemblance to the global distribution of  
338 brGDGTs in lake sediments is evident. Notably, the calibration developed by Martínez-Sosa et  
339 al. (2021) is based on brGDGTs from a global lake dataset.

340

341 Using calibration of Martínez-Sosa's et al. (2021), we reconstructed the surface sediment  
 342 temperature of Gahai lake, resulting in a temperature estimate of 9.4°C. This reconstructed  
 343 temperature closely matches the ice-free season temperature recorded by meteorological  
 344 stations in the Gahai region (8.8°C for May to September). Furthermore, considering the  
 345 significant contribution of autochthonous brGDGTs in Gahai lake, we also attempted to  
 346 reconstruct the Holocene paleotemperature record using previously published lake-specific  
 347 brGDGTs-temperature calibrations (e.g., Günther et al., 2014; Martínez-Sosa et al., 2021;  
 348 Russell et al., 2018; Sun et al., 2011; Wang et al., 2016). As depicted in Fig. S3, most of these  
 349 calibrations exhibit qualitatively similar temperature change patterns when applied to the  
 350 sediment core from Gahai Lake. This similarity arises from their shared same principles, just  
 351 utilizing distinct datasets, resulting in records that display analogous trends but vary in absolute  
 352 temperatures.

353



354

355 **Fig. 4** Comparison of the fractional abundances of tetramethylated, pentamethylated, and  
 356 hexamethylated bGDGTs in sediment core samples from Gahai with lake surface

357 sediments from the Tibetan Plateau (Wang et al., 2016; Günther et al., 2014), East Africa  
358 (Russell et al., 2018), and worldwide (Martínez-Sosa et al., 2021).

359

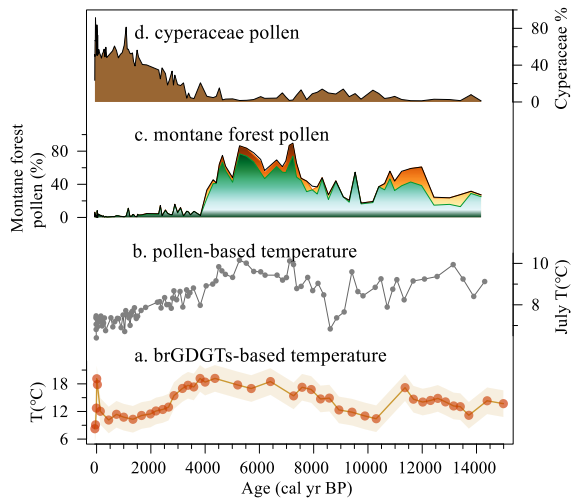
360 The depth interval of 191–279 cm in the Gahai sediment core represents an interval of rapid  
361 allocthonous sedimentation, or alternatively a slump, and therefore the results for the  
362 corresponding time interval of 20–15 ka may be unreliable. Thus, our temperature record of  
363 Months Above Freezing from the eastern TP spans the past 15 ka, with the average temperature  
364 of 4°C, as shown in Fig. 5a. Within the range of age uncertainties, weak warming occurred  
365 during 14.8–11.8 ka, likely to corresponding to the Bølling–Allerød (B/A) interstadial. A minor  
366 cold reversal occurred during 11.8–10.5 ka, potentially corresponding to the Younger Dryas  
367 (YD) event. Notably, the samples collected between 11.8 ka and 10.5 ka exhibited GDGT  
368 concentrations below the detection limit. Therefore, we directly linked the temperature  
369 reconstructions at the two aforementioned time points, ~11.8 ka and ~10.5 ka, resulting in the  
370 lowest temperature of this time period appearing around 10.5 ka. This may cause a time lag  
371 with the occurrence of the YD event. The temperature record indicates a colder period during  
372 11.5–8.0 ka. During 8.0–3.5 ka, Gahai experienced a stable warm period with the average  
373 temperature of ~16.5°C, after which the temperature decreased gradually. Overall, the  
374 maximum temperature difference since 15 ka was ~10°C. As for the absolute temperature  
375 changes since 15,000 yr, although some influential studies indicate a warming of approximately  
376 6.1–7°C from the deglaciation onset to preindustrial times (Tierney et al., 2020; Osman et al.,  
377 2021). However, these results are based on global mean sea surface temperatures. Our  
378 reconstructed temperature range is about 10°C, considering the remarkable ‘elevation-

379 dependent warming' observed in high-altitude regions compared to low-altitude areas  
380 ([Mountain Initiative EDW Working Group, 2015](#)). Thus, this range could be accurate.  
381 Nevertheless, we do not rule out the possibility that our temperature reconstruction may exhibit  
382 an overestimation. Aside from potential uncertainties associated with the biomarkers  
383 themselves, calibrations may also considerably influence the observed amplitude. We  
384 examined temperature variations reconstructed using different calibrations (Fig. S3), with the  
385 smallest range being 6°C and the largest being 12°C. Undoubtedly, further efforts are needed  
386 to constrain the inherent uncertainties related to biomarker-based temperature reconstructions.

387

#### 388 *3.4 Holocene temperature changes on the eastern edge of TP and their origin*

389 Despite the difference in amplitude, the temperature record of Months Above Freezing from  
390 Gahai resembles the pollen record and the pollen-based temperature reconstruction from the  
391 same site (Fig. 5) ([Wang et al., 2022](#)). However, the brGDGTs-based Holocene Thermal  
392 Maximum (HTM) lags the pollen-based reconstruction (Fig. 5a, b). Wang et al. (2022) used a  
393 weighted-averaging partial least regression approach to produce a temperature record for Gahai,  
394 based on a modern pollen dataset (n=731) from the eastern TP. Assessment of the statistical  
395 significance of the pollen-based climate variables for Gahai suggests that the mean July  
396 temperature is the most important environmental factor influencing the fossil pollen  
397 assemblages. The brGDGTs in Gahai are indicative of summer and autumn temperatures, and  
398 the mismatch between the temperature records inferred from brGDGTs and the pollen record  
399 may be attributed to the difference between the solar irradiance during June–October and that  
400 during July. A detailed analysis of this topic will be undertaken in the subsequent section.



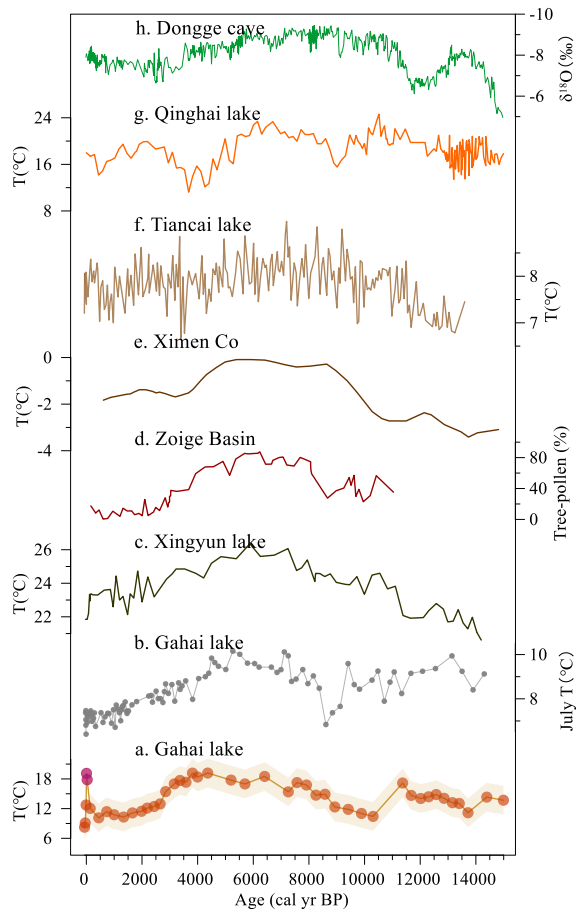
401

402 **Fig. 5** Comparison of multiproxy records from Gahai lake. (a) brGDGTs-based MAF (this  
 403 study). (b) Temperature of the warmest month (July) based on pollen assemblages  
 404 (Wang et al., 2022). (c, d) Pollen-reconstructed montane forest (*Pinus*, *Picea*, *Abies*) and  
 405 Cyperaceae pollen record (Wang et al., 2022).

406

407 The brGDGTs-based temperature record from Gahai confirms the occurrence of a climate  
 408 optimum in the mid-Holocene on the northeast Tibetan Plateau, which is consistent with several  
 409 other pollen and pollen-reconstructed temperature records from the fringe areas of the Asian  
 410 summer monsoon (Fig. 6), suggesting that it is a reliable representation of Holocene  
 411 temperature changes in this region. For example, pollen-based temperature reconstructions  
 412 from Xingyun lake and Ximen Co on the eastern TP show a early to middle HTM (9–4 ka) and  
 413 a cooling trend thereafter (Fig. 6c, e) (Wu et al., 2018; Herzschuh et al., 2014; Wang et al.,  
 414 2021a). Additionally, lake water temperature reconstructions based on subfossil chironomids  
 415 from Tiancai lake (Fig. 6f) (Zhang et al., 2017; Zhang et al., 2019a) and alkenones from

416 Qinghai lake (Fig. 6g) (Hou et al., 2016) show the same trends during the past 15 ka, as also  
417 shown by other pollen-based temperature records from the TP (Chen et al., 2020). Pollen,  
418 chironomids and alkenones mainly respond to the growing season temperatures in middle and  
419 high latitudes, and thus the reconstructed temperature records are consistent with the variations  
420 in summer solar irradiance. Similar variations were documented in temperature reconstructions  
421 at a global scale (Marcott et al., 2013; Cartapanis et al., 2022). Nevertheless, the timing and  
422 amplitude of the Gahai temperature fluctuations differ from those of other temperature records  
423 from this region (Fig. 6). These discrepancies may be the result of the chronological  
424 uncertainties of these records, and related to differences in the seasonal and spatial responses  
425 to climate forcing and feedbacks.



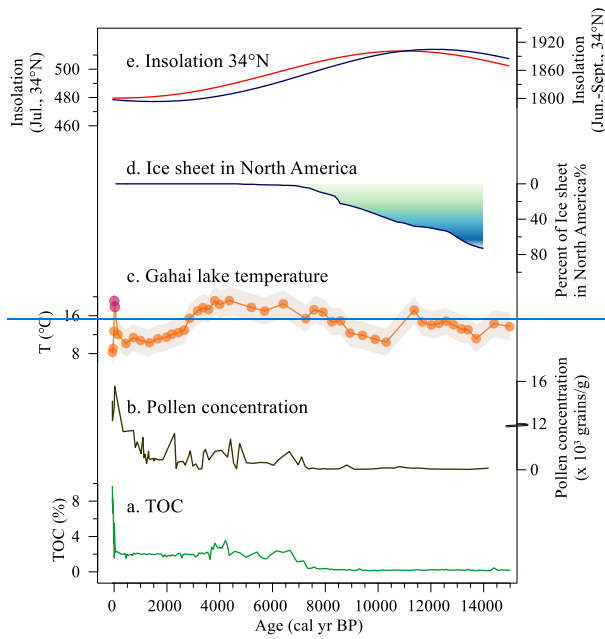
426

427 **Fig. 6** Comparison of temperature at Gahai and other records from the eastern edge of the  
 428 Tibetan Plateau. (a) brGDGTs-based MAF at Gahai, the purple dots may indicate  
 429 unreliable temperature changes influenced by human activities (this study). (b)  
 430 Temperature of the warmest month (July) based on pollen data from Gahai (Wang et al.,  
 431 2022). (c) Pollen-based temperature at Xingyun lake (Wu et al., 2018). (d) Tree pollen  
 432 percentages from the Hongyuan peatland in the southern Zoige Basin (Zhou et al.,  
 433 2010). (e) Pollen-based temperature at Ximen Co (Herzschuh et al., 2014). (f)  
 434 Chironomid-based temperature at Tiancai lake (Zhang et al., 2017, 2019a). (g)  
 435 Alkenone-based temperature at Qinghai lake (Hou et al., 2016). (h) Stalagmite  $\delta^{18}\text{O}$   
 436 record of Dongge cave (Dykoski et al., 2005).

437

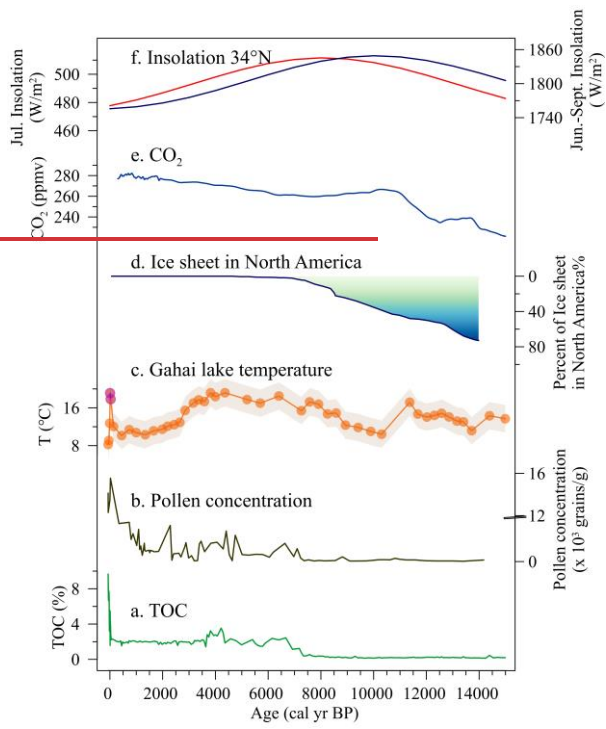
438 Nevertheless, the timing and amplitude of the Gahai temperature fluctuations differ from those  
439 of other temperature records from this region (Fig. 6). These discrepancies may be the result  
440 of the chronological uncertainties of these records, and to differences in the seasonal and spatial  
441 responses to climate forcing and feedbacks. The temperature records shown in Fig. 6 mostly  
442 refer to summer temperatures, which are primarily influenced by summer insolation.

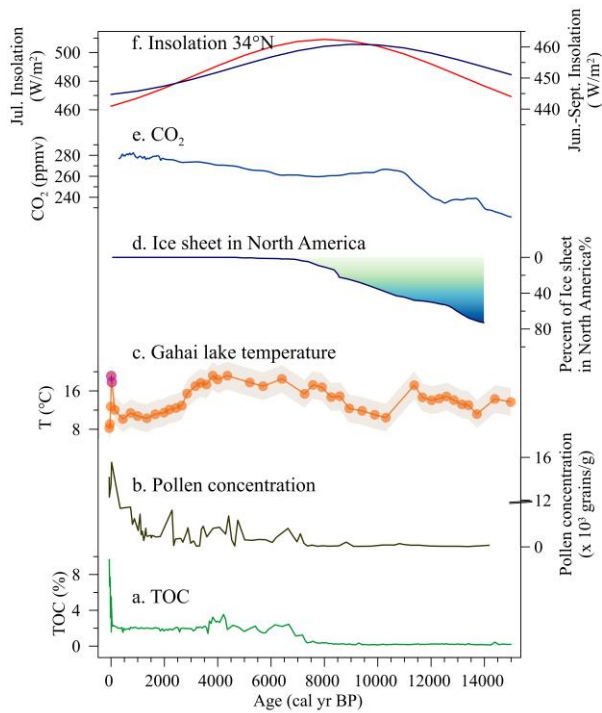
带格式的: 缩进: 左侧: 0 厘米, 首行缩进: 0 字符



443







445  
 446 **Fig. 7** Temperature fluctuations and forcing factors during the Holocene. (a, b) TOC content  
 447 and pollen concentrations from Gahai (Wang et al., 2022). (c) brGDGTs-based MAF  
 448 from Gahai, the purple dots may indicate unreliable temperature changes influenced by  
 449 human activities (this study). (d) Percentage of the remnant Laurentide ice sheet in  
 450 North America relative to the Last Glacial Maximum (Dyke, 2004). (e) [Variation of](#)  
 451 [atmospheric CO<sub>2</sub> content \(Monnin et al., 2004\)](#). (f) [Local insolation at 34 °N during July](#)  
 452 [\(navy blue curve\) and ice-free months \(red curve\) \(Laskar et al., 2004\)](#). [Mean insolation](#)  
 453 [during July \(W/m<sup>2</sup>\) \(navy blue curve\) and mean insolation during ice-free months](#)  
 454 [\(W/m<sup>2</sup>\) at 34 °N \(red curve\) \(Berger and Loutre, 1991; Berger et al., 2010\)](#).

设置了格式：下标

设置了格式：上标

设置了格式：上标

456 The temperature record in Gahai during the early Holocene fails to closely track the Northern  
457 Hemisphere insolation trend, and there is also a time lag. The pollen-based temperature record  
458 for Xingyun Lake in southwestern China also shows lower temperatures in the early Holocene  
459 (Fig. 6c). The albedo effect caused by the increased cloud cover may be the reason for the early  
460 Holocene decrease in summer temperatures (Wu et al., 2018). However, the pollen record from  
461 Gahai indicates dry conditions during the early Holocene (Wang et al., 2022), and cloud cover  
462 may not be the primary factor responsible for the low temperatures at this time. The melting of  
463 Northern Hemisphere ice sheets during the early Holocene would weakened the Atlantic  
464 Meridional Overturning Circulation (AMOC) and potentially also the global thermohaline  
465 circulation. This would ~~led~~ lead to a reduction in the amount of heat transport by the North  
466 Atlantic warm current to high-latitude regions and a cooling in middle to high latitudes of the  
467 Northern Hemisphere, which resulted in the low temperatures in middle to high latitudes of  
468 the Northern Hemisphere. The persistence of the Laurentide ice sheet into the early Holocene  
469 maintained the regional albedo, as well as discharging meltwater into the North Atlantic (Fig.  
470 7d) (Dyke, 2004). Furthermore, the cooling during the early Holocene followed by the warming  
471 trend in the mid-Holocene potentially correlates with significant fluctuations in CO<sub>2</sub>  
472 concentrations within these intervals (Fig. 7e) (Monnin et al., 2004). In addition, a Holocene  
473 temperature simulation showed that global warming was more pronounced when dust factors  
474 were excluded from the simulation (Liu et al. (2018). The record of insoluble particles in the  
475 Greenland GISP2 ice core indicates relatively high concentrations of atmospheric aerosols in  
476 the early Holocene (Zielinski and Mershon, 1997), which would gave weakened summer solar  
477 irradiation via radiative feedback, leading to the cool temperatures during this period. In

设置了格式: 下标

478 [essence, temperature, especially seasonal variations like the Gahai ice-free temperature in the](#)  
479 [eastern TP, is influenced by multifaceted factors including astronomical forcing, CO<sub>2</sub>, and ice](#)  
480 [sheets. Temperature exhibits varied sensitivities in response to these factors, while both](#)  
481 [insolation and CO<sub>2</sub> exert considerable and favorable impacts on summer temperature patterns](#)  
482 (Lyu and Yin, 2022). These factors may together have caused the early Holocene temperature  
483 decline at Gahai Lake, which slightly delayed the onset of the Holocene Warm Period.

设置了格式: 下标

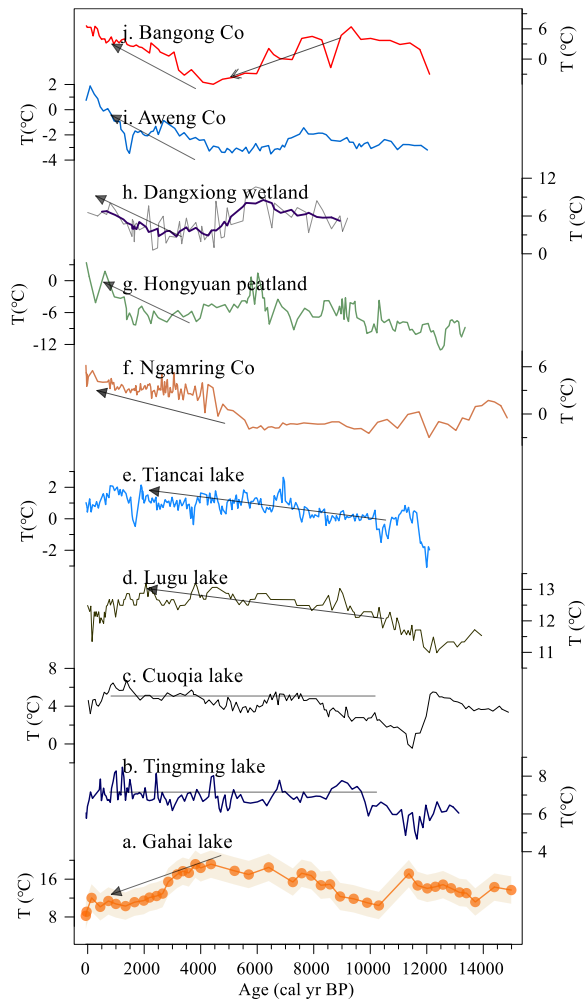
设置了格式: 下标

484  
485 A notable and rapid temperature increase is evident at Gahai in recent decades, which differs  
486 from the other records (Fig. 7c). Moreover, there are notable increases in pollen concentration,  
487 TOC, and TN (Fig. 7a, b) in the Gahai sediment core, indicating intensive local human activities  
488 like grazing and tourism, which may be the primary cause of the environmental changes in this  
489 region (Wang et al., 2022). This intensive human activity may have reduced the ability of the  
490 brGDGTs to record the natural temperature background. These observations emphasize the  
491 important impact of human activities on climate proxies and the need to carefully consider their  
492 effect on temperature reconstructions.

### 493 494 *3.5 Spatiotemporal pattern of brGDGTs-based TP temperatures*

495 In addition to comparing the Gahai temperature with the summer temperature records from the  
496 eastern TP and its surrounding areas, we compiled and reviewed published Holocene  
497 brGDGTs-based quantitative temperature records from across the TP. As shown in Fig. 8, with  
498 the increasing number of these records for the TP, the differences between the results have  
499 become more pronounced. The brGDGTs records from lakes in the central and western parts

500 of the plateau show higher temperatures in the early and late Holocene, and lower temperatures  
501 in the middle Holocene (Wang et al., 2021c; Li et al., 2017; He et al., 2020), while the brGDGTs  
502 records from lakes in the southern and south-eastern parts of the TP show a warming trend  
503 throughout the Holocene (Sun et al., 2022; Feng et al., 2022). In addition, brGDGTs in Cuoqia  
504 lake and Tingming lake, on the south-eastern TP, recorded the ice-free season temperature,  
505 which was relatively stable during the Holocene (Sun et al., 2021; Zhang et al., 2022a).  
506 However, our temperature record from Gahai is different from the above records and resembles  
507 summer temperature changes during the Holocene (Chen et al., 2020). This is because the  
508 brGDGTs record from Lake Gahai represents warm season temperatures, which adds to its  
509 reliability.



510

511 **Fig. 8** Comparison of Holocene temperature based on brGDGTs at Gahai (a) and other  
 512 records from around the TP. Reconstructed ice-free-season temperatures from (b)  
 513 Tingming lake (Sun et al., 2021), (c) Cuoqia lake (Zhang et al., 2022a). Reconstructed  
 514 annual temperature from (d) Lugu lake (Zhao et al., 2021b), (e) Tiancai lake (Feng et al.,  
 515 2022), (f) Ngamring Co (Sun et al., 2022), (g) Hongyuan peatland (Yan et al., 2021). (h)  
 516 Dangxiong wetland (Cheung et al., 2017), (i) Aweng Co (Li et al., 2017), (j) Bangong

517 Co (Wang et al., 2021c).

518

519 We suggest that the complexity of Holocene temperature patterns recorded by brGDGTs in TP  
520 lakes is primarily due to the ambiguity of brGDGTs in these lakes, as well as to the spatial  
521 heterogeneity of climate change across the TP. This ambiguity can be attributed to several  
522 factors. First, the origin of brGDGTs in lakes remains an uncertain factor in temperature  
523 reconstruction. An increasing number of studies indicate the occurrence of a remarkable  
524 amount of autochthonous brGDGTs in lakes, but their abundance in soil can also affect the  
525 distribution of brGDGTs in lakes due to their supply via soil erosion (e.g., Tierney and Russell,  
526 2009; Weber et al., 2015; Wang et al., 2023). In fact, even within the same lake (e.g.,  
527 Tengchongqinghai lake in southwestern China), two studies reached inconsistent conclusions  
528 regarding the origin of brGDGTs (Tian et al., 2019; Zhao et al., 2021b), possibly because the  
529 niches of certain brGDGTs may expand or contract compared to other locations within a lake.  
530 Therefore, it is important to conduct detailed modern process studies to accurately assess the  
531 sources of brGDGTs in lakes, especially with regard to evaluating the proportion of  
532 autochthonous brGDGTs (Wang et al., 2023; Martin et al., 2020). Second, brGDGTs may show  
533 a seasonal signal. Current brGDGTs–temperature calibrations for lakes reflect the annual  
534 average temperature (Sun et al., 2011; De Jonge et al., 2014), as well as the growing season  
535 temperature (Sun et al., 2011; Dang et al., 2018) and the ice-free season temperature (Martínez-  
536 Sosa et al., 2021; Zhang et al., 2022a). Thus, there is no consensus regarding whether the  
537 brGDGTs have a seasonal bias, and it is necessary to conduct continuous, high-resolution  
538 seasonal investigations of lakes on the Tibetan Plateau to comprehensively elucidate the

539 seasonal characteristics of brGDGTs. This can enhance the accuracy of regional temperature  
540 reconstruction and may help reconcile the complex temperature patterns observed on the  
541 Tibetan Plateau. Third, the factors affecting the distribution of brGDGTs in lakes are complex,  
542 including not only temperature, pH and salinity but also oxygen content, water depth, and so  
543 on (Wang et al., 2021b; Wang et al., 2016). The distribution of brGDGTs in lakes is significantly  
544 influenced by the hydrological and physical properties of the lakes, and thus it is necessary to  
545 attain a more comprehensive understanding of the characteristics of the lakes in the study area  
546 and their effects on brGDGTs. Fourth, different brGDGTs–temperature calibrations may lead  
547 to markable differences in both the amplitude and trend of temperature from the same dataset  
548 (Wang et al., 2016; Feng et al., 2019). One reason for this is the deviation between in-situ  
549 measured temperature and atmospheric temperature (Wang et al., 2020). Thus, selecting an  
550 appropriate calibration and attempting to establish a brGDGTs-in situ temperature calibration  
551 are effective means of enhancing the reliability of brGDGTs-based temperature reconstructions.

552

#### 553 **4 Conclusions**

554 We present a quantitative, brGDGTs-based seasonal paleotemperature record over the last 15  
555 ka from the sediments of a shallow lake on the eastern Tibetan Plateau. Our reconstruction  
556 resembles the summer temperature trend, with the Holocene Thermal Maximum occurring  
557 during 8–3.5 ka. There is a lag between our brGDGTs-based reconstruction and pollen-based  
558 ~~July~~ temperature recorded in the same sediment core, indicating a seasonal bias between  
559 different proxies. Since 3.5 ka, the temperature decreased gradually, and the surficial sediments  
560 reliably recorded the warm season temperature during the current period in the Gahai Lake



561 region. However, intensive local human activity during the last century has affected the  
562 distribution of brGDGTs, resulting in temperature deviations recorded by brGDGTs. However,  
563 the implementation of environmental protection policies have reduced this anthropogenic  
564 signal. Our findings help better understand the seasonal signal of brGDGTs in shallow lakes  
565 and provide important data for improving projections of terrestrial climate change at high  
566 elevations.

567

568 We also investigated previously published brGDGTs-based Holocene temperature records on  
569 the TP to determine the pattern of brGDGTs-based temperature changes and the possible causes  
570 of the differences between reconstructions. We emphasize the need for the careful examination  
571 of both the source and behavior of these compounds in lacustrine environments and lake status,  
572 prior to the application of brGDGTs proxies in paleolimnological reconstruction.

573

#### 574 **Data availability**

575 The data used in this study can be obtained from the corresponding author Juzhi Hou  
576 (houjz@itpcas.ac.cn).

577

#### 578 **Author contributions**

579 Xiaohuan Hou did the experiments, analyzed the data and wrote the manuscript. Nannan Wang,  
580 Zhe Sun, Kan Yuan and Xianyong Cao participated in sample collecting and data analysis.  
581 Juzhi Hou designed this study and led the interpretation. All authors commented on and  
582 improved the manuscript.

583

584 **Competing interests**

585 The contact author has declared that none of the authors has any competing interests.

586

587 **Acknowledgements**

588 This work was financially supported by the National Natural Science Foundation of China  
589 (42025103, 41877459) and the Second Tibetan Plateau Scientific Expedition and Research  
590 (2019QZKK0601). We would like to thank Jan Bloemendal for the help with language  
591 editing.

592

593 **References**

- 594
- 595 Berger, A. and Loutre, M. F.: Insolation values for the climate of the last 1000000 years, *Quaternary Science*
- 596 *Reviews*, 10, 297-317, 10.1016/0277-3791(91)90033-q, 1991.
- 597 Berger, A., Loutre, M. F., and Yin, Q. Z.: Total irradiation during any time interval of the year using elliptic
- 598 integrals, *Quaternary Science Reviews*, 29, 1968-1982, 10.1016/j.quascirev.2010.05.007, 2010.
- 599 Bova, S., Rosenthal, Y., Liu, Z., Godad, S. P., and Yan, M.: Seasonal origin of the thermal maxima at the Holocene
- 600 and the last interglacial, *Nature*, 589, 548-553, 10.1038/s41586-020-03155-x, 2021.
- 601 Buckles, L. K., Weijers, J. W. H., Verschuren, D., and Damste, J. S. S.: Sources of core and intact branched
- 602 tetraether membrane lipids in the lacustrine environment: Anatomy of Lake Challa and its catchment, equatorial
- 603 East Africa, *Geochimica Et Cosmochimica Acta*, 140, 106-126, 10.1016/j.gca.2014.04.042, 2014.
- 604 Cao, J., Rao, Z., Shi, F., and Jia, G.: Ice formation on lake surfaces in winter causes warm-season bias of lacustrine
- 605 brGDGT temperature estimates, *Biogeosciences*, 17, 2521-2536, 10.5194/bg-17-2521-2020, 2020.
- 606 Cartapanis, O., Jonkers, L., Moffa-Sanchez, P., Jaccard, S. L., and de Vernal, A.: Complex spatio-temporal
- 607 structure of the Holocene Thermal Maximum, *Nat Commun*, 13, 5662, 10.1038/s41467-022-33362-1, 2022.
- 608 Chen, D., Xu, B., Yao, T., Guo, Z., Cui, P., Chen, F., Zhang, R., Zhang, X., Zhang, Y., Fan, J., Hou, Z., and Zhang,
- 609 T.: Assessment of past, present and future environmental changes on the Tibetan Plateau, *Chinese Science Bulletin*,
- 610 60, 3025-3035, 2015.
- 611 Chen, F., Yu, Z., Yang, M., Ito, E., Wang, S., Madsen, D. B., Huang, X., Zhao, Y., Sato, T., Birks, H. J. B., Boomer,
- 612 I., Chen, J., An, C., and Wünnemann, B.: Holocene moisture evolution in arid central Asia and its out-of-phase
- 613 relationship with Asian monsoon history, *Quaternary Science Reviews*, 27, 351-364,
- 614 10.1016/j.quascirev.2007.10.017, 2008.
- 615 Chen, F., Zhang, J., Liu, J., Cao, X., Hou, J., Zhu, L., Xu, X., Liu, X., Wang, M., Wu, D., Huang, L., Zeng, T.,
- 616 Zhang, S., Huang, W., Zhang, X., and Yang, K.: Climate change, vegetation history, and landscape responses on
- 617 the Tibetan Plateau during the Holocene: A comprehensive review, *Quaternary Science Reviews*, 243,
- 618 10.1016/j.quascirev.2020.106444, 2020.
- 619 Chen, Y., Zheng, F., Yang, H., Yang, W., Wu, R., Liu, X., Liang, H., Chen, H., Pei, H., Zhang, C., Pancost, R. D.,
- 620 and Zeng, Z.: The production of diverse brGDGTs by an Acidobacterium providing a physiological basis for
- 621 paleoclimate proxies, *Geochimica et Cosmochimica Acta*, 337, 155-165, 10.1016/j.gca.2022.08.033, 2022.
- 622 Cheung, M.-C., Zong, Y., Zheng, Z., Liu, Z., and Aitchison, J. C.: Holocene temperature and precipitation
- 623 variability on the central Tibetan Plateau revealed by multiple palaeo-climatic proxy records from an alpine
- 624 wetland sequence, *The Holocene*, 27, 1669-1681, 10.1177/0959683617702225, 2017.
- 625 Committee, L. C. L. C. C.: Luqu County Chronicles, Gansu Cultural Publishing House, Lanzhou, 71 pp.2006.
- 626 Crampton-Flood, E. D., Tierney, J. E., Peterse, F., Kirkels, F. M. S. A., and Damste, J. S. S.: BayMBT: A Bayesian
- 627 calibration model for branched glycerol dialkyl glycerol tetraethers in soils and peats, *Geochimica Et*
- 628 *Cosmochimica Acta*, 268, 142-159, 10.1016/j.gca.2019.09.043, 2020.
- 629 Dang, X., Ding, W., Yang, H., Pancost, R. D., Naafs, B. D. A., Xue, J., Lin, X., Lu, J., and Xie, S.: Different
- 630 temperature dependence of the bacterial brGDGT isomers in 35 Chinese lake sediments compared to that in soils,
- 631 *Organic Geochemistry*, 119, 72-79, 10.1016/j.orggeochem.2018.02.008, 2018.
- 632 De Jonge, C., Hopmans, E. C., Zell, C. I., Kim, J.-H., Schouten, S., and Sinninghe Damsté, J. S.: Occurrence and
- 633 abundance of 6-methyl branched glycerol dialkyl glycerol tetraethers in soils: Implications for palaeoclimate
- 634 reconstruction, *Geochimica et Cosmochimica Acta*, 141, 97-112, 10.1016/j.gca.2014.06.013, 2014.
- 635 Ding, S., Xu, Y., Wang, Y., He, Y., Hou, J., Chen, L., and He, J. S.: Distribution of branched glycerol dialkyl
- 636 glycerol tetraethers in surface soils of the Qinghai-Tibetan Plateau: implications of brGDGTs-based proxies in

设置了格式: 字体: (默认) Times New Roman

637 cold and dry regions, *Biogeosciences*, 12, 3141-3151, 10.5194/bg-12-3141-2015, 2015.

638 Dong, Y., Wu, N., Li, F., Zhang, D., Zhang, Y., Shen, C., and Lu, H.: The Holocene temperature conundrum  
639 answered by mollusk records from East Asia, *Nat Commun*, 13, 5153, 10.1038/s41467-022-32506-7, 2022.

640 Dyke, A. S.: An outline of North American deglaciation with emphasis on central and northern Canada,  
641 Quaternary Glaciations-Extent and Chronology, Pt 2: North America, 2, 373-424, 10.1016/s1571-0866(04)80209-  
642 4, 2004.

643 Dykoski, C. A., Edwards, R. L., Cheng, H., Yuan, D. X., Cai, Y. J., Zhang, M. L., Lin, Y. S., Qing, J. M., An, Z.  
644 S., and Revenaugh, J.: A high-resolution, absolute-dated Holocene and deglacial Asian monsoon record from  
645 Dongge Cave, China, *Earth and Planetary Science Letters*, 233, 71-86, 10.1016/j.epsl.2005.01.036, 2005.

646 Feng, X., Zhao, C., D'Andrea, W. J., Liang, J., Zhou, A., and Shen, J.: Temperature fluctuations during the  
647 Common Era in subtropical southwestern China inferred from brGDGTs in a remote alpine lake, *Earth and*  
648 *Planetary Science Letters*, 510, 26-36, 10.1016/j.epsl.2018.12.028, 2019.

649 Feng, X., Zhao, C., D'Andrea, W. J., Hou, J., Yang, X., Xiao, X., Shen, J., Duan, Y., and Chen, F.: Evidence for a  
650 Relatively Warm Mid-to Late Holocene on the Southeastern Tibetan Plateau, *Geophysical Research Letters*, 49,  
651 10.1029/2022gl098740, 2022.

652 Group, M. I. E. W.: Elevation-dependent warming in mountain regions of the world, *Nature Climate Change*, 5,  
653 424-430, 10.1038/nclimate2563, 2015.

654 Günther, F., Thiele, A., Gleixner, G., Xu, B., Yao, T., and Schouten, S.: Distribution of bacterial and archaeal ether  
655 lipids in soils and surface sediments of Tibetan lakes: Implications for GDGT-based proxies in saline high  
656 mountain lakes, *Organic Geochemistry*, 67, 19-30, 10.1016/j.orggeochem.2013.11.014, 2014.

657 Halamka, T. A., Raberg, J. H., McFarlin, J. M., Younkin, A. D., Mulligan, C., Liu, X. L., and Kopf, S. H.:  
658 Production of diverse brGDGTs by *Acidobacterium Solibacter usitatus* in response to temperature, pH, and O<sub>2</sub>  
659 provides a culturing perspective on brGDGT proxies and biosynthesis, *Geobiology*, 10.1111/gbi.12525, 2022.

660 He, Y., Hou, J., Wang, M., Li, X., Liang, J., Xie, S., and Jin, Y.: Temperature Variation on the Central Tibetan  
661 Plateau Revealed by Glycerol Dialkyl Glycerol Tetraethers From the Sediment Record of Lake Linggo Co Since  
662 the Last Deglaciation, *Frontiers in Earth Science*, 8, 10.3389/feart.2020.574206, 2020.

663 Herzschuh, U., Borkowski, J., Schewe, J., Mischke, S., and Tian, F.: Moisture-advection feedback supports strong  
664 early-to-mid Holocene monsoon climate on the eastern Tibetan Plateau as inferred from a pollen-based  
665 reconstruction, *Palaeogeography, Palaeoclimatology, Palaeoecology*, 402, 44-54, 10.1016/j.palaeo.2014.02.022,  
666 2014.

667 Hou, J., Li, C., and Lee, S.: The temperature record of the Holocene: progress and controversies, *Science Bulletin*,  
668 10.1016/j.scib.2019.02.012, 2019.

669 Hou, J., Huang, Y., Zhao, J., Liu, Z., Colman, S., and An, Z.: Large Holocene summer temperature oscillations  
670 and impact on the peopling of the northeastern Tibetan Plateau, *Geophysical Research Letters*, 43, 1323-1330,  
671 10.1002/2015gl067317, 2016.

672 Huguet, C., Hopmans, E. C., Febo-Ayala, W., Thompson, D. H., Sinninghe Damsté, J. S., and Schouten, S.: An  
673 improved method to determine the absolute abundance of glycerol dibiphytanyl glycerol tetraether lipids, *Organic*  
674 *Geochemistry*, 37, 1036-1041, 10.1016/j.orggeochem.2006.05.008, 2006.

675 Kuang, X. and Jiao, J. J.: Review on climate change on the Tibetan Plateau during the last half century, *Journal of*  
676 *Geophysical Research: Atmospheres*, 121, 3979-4007, 10.1002/2015jd024728, 2016.

677 Laskar, J., Robutel, P., Joutel, F., Gastineau, M., Correia, A. C. M., and Levrard, B.: A long-term numerical  
678 solution for the insolation quantities of the Earth, *Astronomy & Astrophysics*, 428, 261-285, 10.1051/0004-  
679 6361:20041335, 2004.

680 Li, X., Wang, M., Zhang, Y., Lei, L., and Hou, J.: Holocene climatic and environmental change on the western

设置了格式: 字体: (默认) Times New Roman

设置了格式: 字体: (默认) Times New Roman

681 Tibetan Plateau revealed by glycerol dialkyl glycerol tetraethers and leaf wax deuterium-to-hydrogen ratios at  
682 Aweng Co, Quaternary Research, 87, 455-467, 10.1017/qua.2017.9, 2017.

683 Liu, Y., Zhang, M., Liu, Z., Xia, Y., Huang, Y., Peng, Y., and Zhu, J.: A Possible Role of Dust in Resolving the  
684 Holocene Temperature Conundrum, Scientific Reports, 8, 10.1038/s41598-018-22841-5, 2018.

685 Liu, Z. Y., Zhu, J., Rosenthal, Y., Zhang, X., Otto-Bliesner, B. L., Timmermann, A., Smith, R. S., Lohmann, G.,  
686 Zheng, W. P., and Timm, O. E.: The Holocene temperature conundrum, Proc. Natl. Acad. Sci. U. S. A., 111, E3501-  
687 E3505, 10.1073/pnas.1407229111, 2014.

688 Loomis, S. E., Russell, J. M., Heureux, A. M., D'Andrea, W. J., and Sinninghe Damsté, J. S.: Seasonal variability  
689 of branched glycerol dialkyl glycerol tetraethers (brGDGTs) in a temperate lake system, Geochimica et  
690 Cosmochimica Acta, 144, 173-187, 10.1016/j.gca.2014.08.027, 2014.

691 Lu, H., Wu, N., Liu, K.-b., Zhu, L., Yang, X., Yao, T., Wang, L., Li, Q., Liu, X., Shen, C., Li, X., Tong, G., and  
692 Jiang, H.: Modern pollen distributions in Qinghai-Tibetan Plateau and the development of transfer functions for  
693 reconstructing Holocene environmental changes, Quaternary Science Reviews, 30, 947-966,  
694 10.1016/j.quascirev.2011.01.008, 2011.

695 Lyu, A. and Yin, Q. Z.: The spatial-temporal patterns of East Asian climate in response to insolation, CO<sub>2</sub> and ice  
696 sheets during MIS-5, Quaternary Science Reviews, 293, 10.1016/j.quascirev.2022.107689, 2022.

697 Ma, W., Li, G., Song, J., Yan, L., and Wu, L.: Effect of Vegetation Degradation on Soil Organic Carbon Pool and  
698 Carbon Pool Management Index in the Gahai Wetland, China, Acta Agraria Sinica, 27, 687-694, 2019.

699 Marcott, S. A., Shakun, J. D., Clark, P. U., and Mix, A. C.: A Reconstruction of Regional and Global Temperature  
700 for the Past 11,300 Years, Science, 339, 1198-1201, 10.1126/science.1228026, 2013.

701 Marsicek, J., Shuman, B. N., Bartlein, P. J., Shafer, S. L., and Brewer, S.: Reconciling divergent trends and  
702 millennial variations in Holocene temperatures, Nature, 554, 92-+, 10.1038/nature25464, 2018.

703 Martin, C., Ménot, G., Thouveny, N., Peyron, O., Andrieu-Ponel, V., Montade, V., Davtian, N., Reille, M., and  
704 Bard, E.: Early Holocene Thermal Maximum recorded by branched tetraethers and pollen in Western Europe  
705 (Massif Central, France), Quaternary Science Reviews, 228, 106109, 10.1016/j.quascirev.2019.106109, 2020.

706 Martínez-Sosa, P., Tierney, J. E., Stefanescu, I. C., Dearing Crampton-Flood, E., Shuman, B. N., and Routson, C.:  
707 A global Bayesian temperature calibration for lacustrine brGDGTs, Geochimica et Cosmochimica Acta, 305, 87-  
708 105, 10.1016/j.gca.2021.04.038, 2021.

709 Monnin, E., Steig, E. J., Siegenthaler, U., Kawamura, K., Schwander, J., Stauffer, B., Stocker, T. F., Morse, D. L.,  
710 Barnola, J. M., Bellier, B., Raynaud, D., and Fischer, H.: Evidence for substantial accumulation rate variability in  
711 Antarctica during the Holocene, through synchronization of CO<sub>2</sub> in the Taylor Dome, Dome C and DML ice cores,  
712 Earth and Planetary Science Letters, 224, 45-54, 10.1016/j.epsl.2004.05.007, 2004.

713 Moser, K. A., Baron, J. S., Brahney, J., Oleksy, I. A., Saros, J. E., Hundey, E. J., Sadro, S., Kopáček, J., Sommaruga,  
714 R., Kainz, M. J., Strecker, A. L., Chandra, S., Walters, D. M., Preston, D. L., Michelutti, N., Lepori, F., Spaulding,  
715 S. A., Christianson, K. R., Melack, J. M., and Smol, J. P.: Mountain lakes: Eyes on global environmental change,  
716 Global and Planetary Change, 178, 77-95, 10.1016/j.gloplacha.2019.04.001, 2019.

717 Opitz, S., Zhang, C., Herzsuh, U., and Mischke, S.: Climate variability on the south-eastern Tibetan Plateau  
718 since the Lateglacial based on a multiproxy approach from Lake Naleng – comparing pollen and non-pollen  
719 signals, Quaternary Science Reviews, 115, 112-122, 10.1016/j.quascirev.2015.03.011, 2015.

720 Osman, M. B., Tierney, J. E., Zhu, J., Tardif, R., Hakim, G. J., King, J., and Poulsen, C. J.: Globally resolved  
721 surface temperatures since the Last Glacial Maximum, Nature, 599, 239-244, 10.1038/s41586-021-03984-4, 2021.

722 Pang, H., Hou, S., Zhang, W., Wu, S., Jenk, T. M., Schwikowski, M., and Jouzel, J.: Temperature Trends in the  
723 Northwestern Tibetan Plateau Constrained by Ice Core Water Isotopes Over the Past 7,000 Years, Journal of  
724 Geophysical Research-Atmospheres, 125, 10.1029/2020jd032560, 2020.

725 Qiu, J.: The third pole, *Nature*, 454, 393-396, 10.1038/454393a, 2008.

726 Russell, J. M., Hopmans, E. C., Loomis, S. E., Liang, J., and Sinninghe Damsté, J. S.: Distributions of 5- and 6-  
727 methyl branched glycerol dialkyl glycerol tetraethers (brGDGTs) in East African lake sediment: Effects of  
728 temperature, pH, and new lacustrine paleotemperature calibrations, *Organic Geochemistry*, 117, 56-69,  
729 10.1016/j.orggeochem.2017.12.003, 2018.

730 Sinninghe Damsté, J. S., Hopmans, E. C., Pancost, R. D., Schouten, S., and Geenevasen, J. A. J.: Newly discovered  
731 non-isoprenoid glycerol dialkyl glycerol tetraether lipids in sediments, *Chemical Communications*, 1683-1684,  
732 10.1039/b004517i, 2000.

733 Sinninghe Damsté, J. S., Ossebaar, J., Abbas, B., Schouten, S., and Verschuren, D.: Fluxes and distribution of  
734 tetraether lipids in an equatorial African lake: Constraints on the application of the TEX86 palaeothermometer  
735 and BIT index in lacustrine settings, *Geochimica et Cosmochimica Acta*, 73, 4232-4249,  
736 10.1016/j.gca.2009.04.022, 2009.

737 Sun, Q., Chu, G., Liu, M., Xie, M., Li, S., Ling, Y., Wang, X., Shi, L., Jia, G., and Lü, H.: Distributions and  
738 temperature dependence of branched glycerol dialkyl glycerol tetraethers in recent lacustrine sediments from  
739 China and Nepal, *Journal of Geophysical Research*, 116, 10.1029/2010jg001365, 2011.

740 Sun, X., Zhao, C., Zhang, C., Feng, X., Yan, T., Yang, X., and Shen, J.: Seasonality in Holocene Temperature  
741 Reconstructions in Southwestern China, *Paleoceanography and Paleoclimatology*, 36, 10.1029/2020pa004025,  
742 2021.

743 Sun, Z., Hou, X., Ji, K., Yuan, K., Li, C., Wang, M., and Hou, J.: Potential winter-season bias of annual temperature  
744 variations in monsoonal Tibetan Plateau since the last deglaciation, *Quaternary Science Reviews*, 292,  
745 10.1016/j.quascirev.2022.107690, 2022.

746 Thompson, L. G., Yao, T., Davis, M. E., Henderson, K. A., MosleyThompson, E., Lin, P. N., Beer, J., Synal, H.  
747 A., ColeDai, J., and Bolzan, J. F.: Tropical climate instability: The last glacial cycle from a Qinghai-Tibetan ice  
748 core, *Science*, 276, 1821-1825, 10.1126/science.276.5320.1821, 1997.

749 Tian, L., Wang, M., Zhang, X., Yang, X., Zong, Y., Jia, G., Zheng, Z., and Man, M.: Synchronous change of  
750 temperature and moisture over the past 50 ka in subtropical southwest China as indicated by biomarker records in  
751 a crater lake, *Quaternary Science Reviews*, 212, 121-134, 10.1016/j.quascirev.2019.04.003, 2019.

752 Tierney, J. E. and Russell, J. M.: Distributions of branched GDGTs in a tropical lake system: Implications for  
753 lacustrine application of the MBT/CBT paleoproxy, *Organic Geochemistry*, 40, 1032-1036,  
754 10.1016/j.orggeochem.2009.04.014, 2009.

755 Tierney, J. E., Russell, J. M., Eggermont, H., Hopmans, E. C., Verschuren, D., and Sinninghe Damsté, J. S.:  
756 Environmental controls on branched tetraether lipid distributions in tropical East African lake sediments,  
757 *Geochimica et Cosmochimica Acta*, 74, 4902-4918, 10.1016/j.gca.2010.06.002, 2010.

758 Tierney, J. E., Zhu, J., King, J., Malevich, S. B., Hakim, G. J., and Poulsen, C. J.: Glacial cooling and climate  
759 sensitivity revisited, *Nature*, 584, 569-+, 10.1038/s41586-020-2617-x, 2020.

760 van Bree, L. G. J., Peterse, F., Baxter, A. J., De Crop, W., van Grinsven, S., Villanueva, L., Verschuren, D., and  
761 Sinninghe Damsté, J. S.: Seasonal variability and sources of in situ brGDGT production in a permanently stratified  
762 African crater lake, *Biogeosciences*, 17, 5443-5463, 10.5194/bg-17-5443-2020, 2020.

763 Wang, G., Wang, Y., Wei, Z., He, W., Ma, X., and Zhang, T.: Reconstruction of temperature and precipitation  
764 spanning the past 28 kyr based on branched tetraether lipids from Qionghai Lake, southwestern China,  
765 *Palaeogeography Palaeoclimatology Palaeoecology*, 562, 10.1016/j.palaeo.2020.110094, 2021a.

766 Wang, H., An, Z., Lu, H., Zhao, Z., and Liu, W.: Calibrating bacterial tetraether distributions towards in situ soil  
767 temperature and application to a loess-paleosol sequence, *Quaternary Science Reviews*, 231,  
768 10.1016/j.quascirev.2020.106172, 2020.

769 Wang, H., Chen, W., Zhao, H., Cao, Y., Hu, J., Zhao, Z., Cai, Z., Wu, S., Liu, Z., and Liu, W.: Biomarker-based  
770 quantitative constraints on maximal soil-derived brGDGTs in modern lake sediments, *Earth and Planetary Science*  
771 *Letters*, 602, 10.1016/j.epsl.2022.117947, 2023.

772 Wang, H., Liu, W., He, Y., Zhou, A., Zhao, H., Liu, H., Cao, Y., Hu, J., Meng, B., Jiang, J., Kolpakova, M.,  
773 Krivonogov, S., and Liu, Z.: Salinity-controlled isomerization of lacustrine brGDGTs impacts the associated  
774 MBT5ME' terrestrial temperature index, *Geochimica et Cosmochimica Acta*, 305, 33-48,  
775 10.1016/j.gca.2021.05.004, 2021b.

776 Wang, M., Liang, J., Hou, J., and Hu, L.: Distribution of GDGTs in lake surface sediments on the Tibetan Plateau  
777 and its influencing factors, *Science China Earth Sciences*, 59, 961-974, 10.1007/s11430-015-5214-3, 2016.

778 Wang, M. D., Hou, J. Z., Duan, Y. W., Chen, J. H., Li, X. M., He, Y., Lee, S. Y., and Chen, F. H.: Internal feedbacks  
779 forced Middle Holocene cooling on the Qinghai-Tibetan Plateau, *Boreas*, 10.1111/bor.12531, 2021c.

780 Wang, N., Liu, L., Hou, X., Zhang, Y., Wei, H., and Cao, X.: Palynological evidence reveals an arid early Holocene  
781 for the northeast Tibetan Plateau, *Climate of the Past*, 18, 2381-2399, 10.5194/cp-18-2381-2022, 2022.

782 Weber, Y., De Jonge, C., Rijpstra, W. I. C., Hopmans, E. C., Stadnitskaia, A., Schubert, C. J., Lehmann, M. F.,  
783 Sinninghe Damsté, J. S., and Niemann, H.: Identification and carbon isotope composition of a novel branched  
784 GDGT isomer in lake sediments: Evidence for lacustrine branched GDGT production, *Geochimica et*  
785 *Cosmochimica Acta*, 154, 118-129, 10.1016/j.gca.2015.01.032, 2015.

786 Weber, Y., Sinninghe Damsté, J. S., Zopfi, J., De Jonge, C., Gilli, A., Schubert, C. J., Lepori, F., Lehmann, M. F.,  
787 and Niemann, H.: Redox-dependent niche differentiation provides evidence for multiple bacterial sources of  
788 glycerol tetraether lipids in lakes, *Proc Natl Acad Sci U S A*, 115, 10926-10931, 10.1073/pnas.1805186115, 2018.

789 Weijers, J. W. H., Schouten, S., van den Donker, J. C., Hopmans, E. C., and Sinninghe Damsté, J. S.:  
790 Environmental controls on bacterial tetraether membrane lipid distribution in soils, *Geochimica et Cosmochimica*  
791 *Acta*, 71, 703-713, 10.1016/j.gca.2006.10.003, 2007.

792 Woltering, M., Werne, J. P., Kish, J. L., Hicks, R., Sinninghe Damsté, J. S., and Schouten, S.: Vertical and temporal  
793 variability in concentration and distribution of thaumarchaeotal tetraether lipids in Lake Superior and the  
794 implications for the application of the TEX86 temperature proxy, *Geochimica et Cosmochimica Acta*, 87, 136-  
795 153, 10.1016/j.gca.2012.03.024, 2012.

796 Wu, D., Chen, X., Lv, F., Brenner, M., Curtis, J., Zhou, A., Chen, J., Abbott, M., Yu, J., and Chen, F.: Decoupled  
797 early Holocene summer temperature and monsoon precipitation in southwest China, *Quaternary Science Reviews*,  
798 193, 54-67, 10.1016/j.quascirev.2018.05.038, 2018.

799 Wu, J., Yang, H., Pancost, R. D., Naafs, B. D. A., Qian, S., Dang, X., Sun, H., Pei, H., Wang, R., Zhao, S., and  
800 Xie, S.: Variations in dissolved O<sub>2</sub> in a Chinese lake drive changes in microbial communities and impact  
801 sedimentary GDGT distributions, *Chemical Geology*, 579, 10.1016/j.chemgeo.2021.120348, 2021.

802 Yan, T., Zhao, C., Yan, H., Shi, G., Sun, X., Zhang, C., Feng, X., and Leng, C.: Elevational differences in Holocene  
803 thermal maximum revealed by quantitative temperature reconstructions at ~30° N on eastern Tibetan Plateau,  
804 *Palaeogeography, Palaeoclimatology, Palaeoecology*, 570, 110364, 10.1016/j.palaeo.2021.110364, 2021.

805 Yao, T., Bolch, T., Chen, D., Gao, J., Immerzeel, W., Piao, S., Su, F., Thompson, L., Wada, Y., Wang, L., Wang,  
806 T., Wu, G., Xu, B., Yang, W., Zhang, G., and Zhao, P.: The imbalance of the Asian water tower, *Nature Reviews*  
807 *Earth & Environment*, 3, 618-632, 10.1038/s43017-022-00299-4, 2022.

808 Zhang, C., Zhao, C., Yu, S.-Y., Yang, X., Cheng, J., Zhang, X., Xue, B., Shen, J., and Chen, F.: Seasonal imprint  
809 of Holocene temperature reconstruction on the Tibetan Plateau, *Earth-Science Reviews*, 226, 103927,  
810 10.1016/j.earscirev.2022.103927, 2022a.

811 Zhang, E., Chang, J., Shulmeister, J., Langdon, P., Sun, W., Cao, Y., Yang, X., and Shen, J.: Summer temperature  
812 fluctuations in Southwestern China during the end of the LGM and the last deglaciation, *Earth and Planetary*

813 Science Letters, 509, 78-87, 10.1016/j.epsl.2018.12.024, 2019a.  
814 Zhang, E., Chang, J., Cao, Y., Sun, W., Shulmeister, J., Tang, H., Langdon, P. G., Yang, X., and Shen, J.: Holocene  
815 high-resolution quantitative summer temperature reconstruction based on subfossil chironomids from the  
816 southeast margin of the Qinghai-Tibetan Plateau, Quaternary Science Reviews, 165, 1-12,  
817 10.1016/j.quascirev.2017.04.008, 2017.  
818 Zhang, G., Luo, W., Chen, W., and Zheng, G.: A robust but variable lake expansion on the Tibetan Plateau, Science  
819 Bulletin, 64, 1306-1309, 10.1016/j.scib.2019.07.018, 2019b.  
820 Zhang, W., Wu, H., Cheng, J., Geng, J., Li, Q., Sun, Y., Yu, Y., Lu, H., and Guo, Z.: Holocene seasonal temperature  
821 evolution and spatial variability over the Northern Hemisphere landmass, Nat Commun, 13, 5334,  
822 10.1038/s41467-022-33107-0, 2022b.  
823 Zhao, B., Castaneda, I. S., Bradley, R. S., Salacup, J. M., de Wet, G. A., Daniels, W. C., and Schneider, T.:  
824 Development of an in situ branched GDGT calibration in Lake 578, southern Greenland, Organic Geochemistry,  
825 152, 10.1016/j.orggeochem.2020.104168, 2021a.  
826 Zhao, C., Liu, Z. H., Rohling, E. J., Yu, Z. C., Liu, W. G., He, Y. X., Zhao, Y., and Chen, F. H.: Holocene  
827 temperature fluctuations in the northern Tibetan Plateau, Quaternary Research, 80, 55-65,  
828 10.1016/j.yqres.2013.05.001, 2013.  
829 Zhao, C., Rohling, E. J., Liu, Z., Yang, X., Zhang, E., Cheng, J., Liu, Z., An, Z., Yang, X., Feng, X., Sun, X.,  
830 Zhang, C., Yan, T., Long, H., Yan, H., Yu, Z., Liu, W., Yu, S.-Y., and Shen, J.: Possible obliquity-forced warmth  
831 in southern Asia during the last glacial stage, Science Bulletin, 66, 1136-1145, 10.1016/j.scib.2020.11.016, 2021b.  
832 Zheng, Y., Li, Q., Wang, Z., Naafs, B. D. A., Yu, X., and Pancost, R. D.: Peatland GDGT records of Holocene  
833 climatic and biogeochemical responses to the Asian Monsoon, Organic Geochemistry, 87, 86-95,  
834 10.1016/j.orggeochem.2015.07.012, 2015.  
835 Zhou, W., Yu, S.-Y., Burr, G. S., Kukla, G. J., Jull, A. J. T., Xian, F., Xiao, J., Colman, S. M., Yu, H., Liu, Z., and  
836 Kong, X.: Postglacial changes in the Asian summer monsoon system: a pollen record from the eastern margin of  
837 the Tibetan Plateau, Boreas, 39, 528-539, 10.1111/j.1502-3885.2010.00150.x, 2010.  
838 Zielinski, G. A. and Mershon, G. R.: Paleoenvironmental implications of the insoluble microparticle record in the  
839 GISP2 (Greenland) ice core during the rapidly changing climate of the Pleistocene-Holocene transition,  
840 Geological Society of America Bulletin, 109, 547-559, 10.1130/0016-7606(1997)109<0547:piotim>2.3.co;2,  
841 1997.

842

843